A simple model for fatigue crack growth in concrete applied to a hinge beam model

Skar, Asmus; Poulsen, Peter Noe; Olesen, John Forbes

Published in:
Engineering Fracture Mechanics

Link to article, DOI:
10.1016/j.engfracmech.2017.06.018

Publication date:
2017

Document Version
Peer reviewed version

A simple model for fatigue crack growth in concrete applied to a hinge beam model

Asmus Skar[1,*]

COWI A/S, Parallelvej 2, 2800 Kgs. Lyngby, Denmark

Peter Noe Poulsen[2], John Forbes Olesen[2]

Technical University of Denmark, Brovej, Building 118, 2800 Kgs. Lyngby, Denmark

Abstract

In concrete structures, fatigue is one of the major causes of material deterioration. Repeated loads result in formation of cracks. Propagation of these cracks cause internal progressive damage within the concrete material which ultimately leads to failure. This paper presents a simplified general concept for non-linear analysis of concrete subjected to cyclic loading. The model is based on the fracture mechanics concepts of the fictitious crack model, considering a fiber of concrete material, and a simple energy based approach for estimating the bridging stress under cyclic loading. Further, the uni-axial fiber response is incorporated in a numerical hinge model for beam analysis. Finally, the hinge model is implemented into a finite element beam element on a constitutive level. The proposed model is compared to experimental results on both fiber- and beam level. The proposed model shows good performance and seems well suited for the description of fatigue crack growth in concrete.

Keywords: Fracture mechanics, cyclic cohesive crack, non-linear FEM, fatigue, concrete

*Corresponding author

Email address: asch@cowi.com (Asmus Skar)

[1]Industrial researcher, PhD

[2]Associate Professor

1. Introduction

Concrete structures, e.g. concrete bridges and rigid or semi-rigid pavements, are subjected to cyclic loading from moving vehicles. This type of loading results in initiation of bending cracks in the quasi-brittle cemented material. Subsequently, these cracks propagate, leading to failure of the structure. The cyclic behaviour of concrete materials has mainly been studied subjected to fatigue loading in direct tensile, flexural or indirect tensile loading, see e.g. Cornelissen [1]. These types of experiments have typically been used to establish *Wöhler* type of fatigue relationships, or so-called S-N curves, and provide some information about the number of cycles to failure and the damage development. However, these tests do not distinguish between crack initiation and crack propagation or elastic and inelastic work.

Slowik et al. [2] stated that damage mainly occurs in the micro-cracked zone present at the tip of a crack. Moreover, they showed that peaks in the loading history enlarge the fracture process zone and accelerate fatigue crack propagation. This observation underlines the importance of studying concrete material behaviour after crack initiation and damage that occurs in the fracture process zone, i.e. deterioration of the aggregate bridging stress during cyclic loading. Reduction of aggregate bridging stress in plain concrete under cyclic uni-axial tension was investigated experimentally by Gylltoft [3], Gopalaratnam and Shah [4], Reinhardt et al. [5], Hordijk [6], Plizzari et al. [7], Toumi et al. [8] and Kessler-Kramer et al. [9]. Zhang et al. [10, 11] performed similar experiments on plain and fiber reinforced concrete. This work resulted in several analytically stress-based models for low-cyclic analysis [12, 13, 14, 6]. These models describe the successive reduction of bridging stress as a consequence of a fatigue process. However, in these models the damaging effect from inner loops below the monotonic curve is neglected.

Elias and Le [15] applied the cyclic cohesive zone model proposed by Nguyen et al. [16] to simulate the tension regime in *Mode I* crack growth in quasi-brittle materials under compressive fatigue. In such cyclic cohesive models, irreversible damage accumulation is controlled by an explicit damage evolution equation where an endurance limit can be incorporated. While in monotonic cohesive zone models mentioned above, the damage state is uniquely defined by the maximum separation attained during the loading history, cyclic cohesive zone models need a more general damage variable. In the literature, stiffness-type [16], separation type [17] and micro-mechanically

motivated damage variables [18] are suggested. For visualization purpose, Ortiz and Pandolfi [19] proposed an energy based conversion of a separation-type damage variable into the range between zero and one. While in the cohesive zone model in [19], the cohesive potential amounts to the work done in a monotonic loading process starting at the origin up to the current maximum separation, Roth et al. [20] suggested that the cohesive potential should be interpreted as a measure of the reversible or stored energy. A review of cyclic cohesive zone models published in the literature is given in Kuna and Roth [21]. Although these cyclic cohesive zone models seems promising for describing the fatigue crack growth in quasi-brittle materials, the models published are complex and typically result in a large number of model parameters.

In order to create a simple and robust modelling framework for engineering application, this paper presents a multi-scale cyclic cohesive model. The model is based on the fracture mechanics concepts of the fictitious crack model [22]. At the lowest level a fiber of concrete material including a crack is considered and a stress-mean strain relationship is established. The cyclic behaviour of the crack is incorporated into the fiber response considering the loading process below the monotonic curve, i.e. fatigue crack growth after crack initiation. Reduction of the bridging stress during cyclic loading is determined applying an energy based approach, relating damage of the cohesive potential to the accumulated work during the fatigue loading process.

For structural analysis of concrete beams, the fiber stress-mean strain relationship is incorporated in a hinge as proposed by Skar et al. [23]. Hinge models have been effectively applied for studying crack growth phenomenon in both plain concrete beams [24, 25, 26, 27], as well as reinforced and fiber-reinforced concrete beams [28, 10, 29, 30, 31]. For the hinge, which is a finite part of the beam, a relationship between the generalized sectional forces and strains is established. The hinge model is then applied as a constitutive model in a non-linear beam element as first proposed by Olesen and Poulsen [32]. Although the underlying description of the hinge is based on the formation of discrete cracks the constitutive behaviour of the hinge is smeared (smooth). This particular feature is practical and effective as it requires no a-priori knowledge of the crack pattern. Skar et al. [33] showed that this model is able to predict the stress distribution and stiffness during crack development, resulting in a precise prediction of the crack-opening.

This paper presents a simple and effective concept for simulating fatigue crack growth in concrete applying an energy based approach for the hinge

fiber response, i.e at the lowest level. The model is incorporated in a hinge for analysis of bending fracture of concrete beams. Further, the hinge model is implemented in a finite element beam element. The presented model represent an extension and generalization compared to previous hinge models, see e.g. [23], accounting for the material behaviour in all the cracked phases, linking the development of the fracture process zone and damage of the existing fracture process zone to the monotonic material characteristics in a rational manner.

2. Energy based cyclic cohesive model

The fatigue crack growth process in concrete may be divided into a crack initiation phase and a crack development phase. In the present study a simple and general format is sought with regard to the fatigue life prediction after crack initiation. This means that the maximum stress σ_{max} at some point has reached the tensile strength f_t, where a crack in the concrete material has initiated. Although a general format is presented, suitable for description of complex pre-peak and post-peak behaviour, the model is simplified for the purpose of studying damage that occurs in the fracture process zone.

The uni-axial tensile behaviour of the concrete material is modelled according to the fictitious crack model by Hillerborg et al. [22]. The linear elastic pre-crack state is described by the elastic modulus, E_c. The uni-axial tensile strength is denoted by f_t and the corresponding strain by ε_{ct}. For simplicity, the stress-crack opening relationship, or so-called softening curve, is given as a linear curve

$$\sigma\left(w\right) = \begin{cases} f_t + aw & \text{for} \quad 0 < w \leq w_c \\ 0 & \text{for} \quad w_c \leq w \end{cases} \tag{1}$$

where a is the negative slope on the softening curve and w is the crack opening. The fracture energy, G_F, is given by the area under the softening curve. The zero-stress crack opening is given as $w_c = 2G_F/f_t$.

The present study aims at creating a simple modelling framework for engineering design purpose, and not models that exactly describes the concrete unloading-reloading hysteresis loops found from experiments, see e.g. Hordijk [6]. For simplicity unloading towards origin is assumed as a starting point for the model development, as shown in Figure 1.

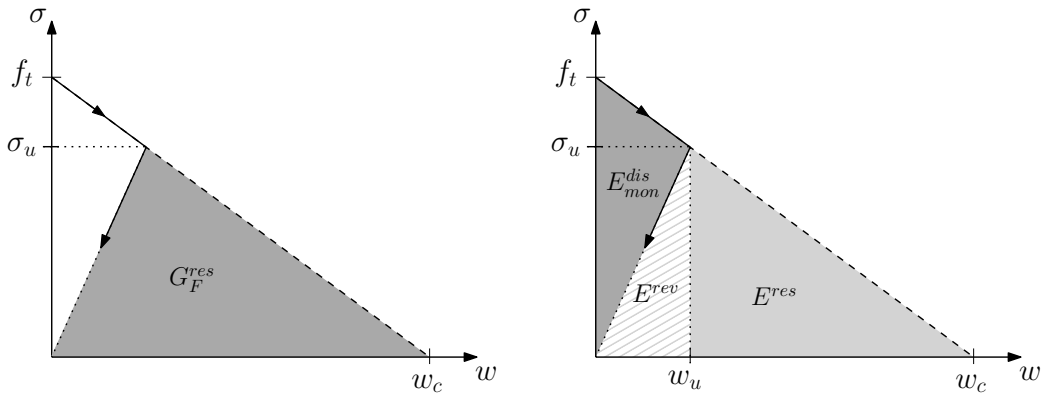

Figure 1: Energy considerations used for description of cyclic behaviour of concrete material in uni-axial tension at the start of fatigue analysis: (a) Residual fracture energy and (b) Dissipated, reversible and residual energy

The cohesive potential, i.e. the residual fracture energy, G_F^{res}, at the point where a fiber of concrete material enters the fatigue phase is given as, see Figure 1 (a),

$$G_F^{res} = G_F - E_{mon}^{dis} = E^{rev} + E^{res} \tag{2}$$

where E_{mon}^{dis} is the dissipated energy from monotonic crack-opening process, E^{rev} is the reversible elastic fracture energy upon the first load cycle and E^{res} is the residual fracture energy upon the first load cycle. These measures can be found from the following expressions, see Figure 1 (b),

$$E^{rev} = \frac{1}{2}\sigma_u w_u \tag{3a}$$

$$E_{mon}^{dis} = \int_0^{w_u} \sigma\left(w\right)\,\mathrm{d}w - E^{rev} = \frac{1}{2}f_t w_u \tag{3b}$$

$$E^{res} = \int_{w_u}^{w_c} \sigma\left(w\right)\,\mathrm{d}w = \frac{1}{2}\sigma_u\left(w_c - w_u\right) \tag{3c}$$

where w_u is the crack-opening at the onset of unloading, σ_u is the stress at the onset of unloading and w_c is the final zero-stress crack-opening.

In incremental unloading-reloading schemes, shown in the grey curve on Figure 2 (a), the gradient at the onset of unloading would decline with decreasing stress level due to the incremental deterioration of the fracture energy. Similarly, the gradient at the onset of reloading, would be equal to the final unloading stiffness, and then decline with increasing stress level. In the model presented here, a more simplified format is selected, assuming a constant unloading and reloading stiffness, i.e. unloading towards origin and reloading towards a fixed point on the monotonic curve, respectively. The fixed point on the monotonic curve is controlled by the residual fracture energy, G_F^{res}, after a cyclic loading process. The residual fracture energy is updated at the onset of reloading. This means, that for a fiber that fails in fatigue, the evolving damage contribution from the final reloading cycle is neglected. However, in general this error will be small, as typically several load cycles, each with a low damage contribution are considered in fatigue. This is exemplified for the reloading process A-B in Figure 2 (a), comparing the simple constant stiffness scheme proposed (black line) and incremental stiffness scheme (gray line) where the deterioration is exaggerated.

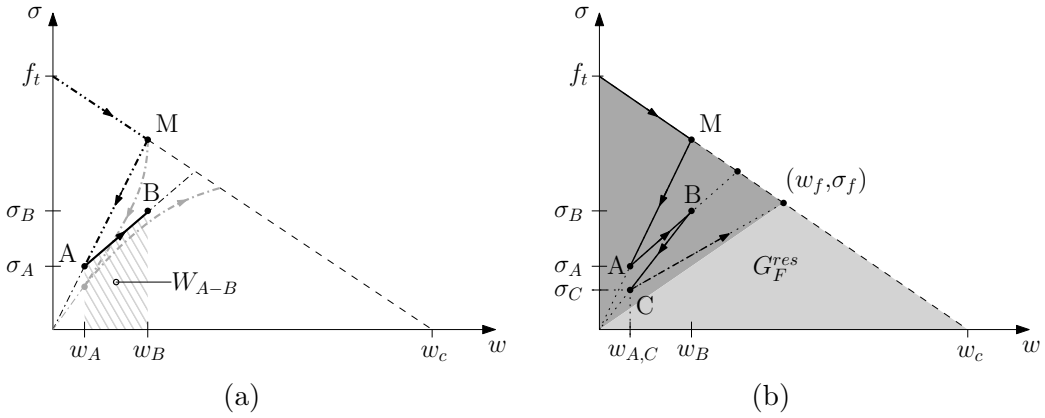

Figure 2: (a) Proposed simplified constant stiffness scheme (black line) compared to a more realistic incremental stiffness scheme (gray line) showing the work of the cyclic reloading process A-B (shaded gray). (b) Sketch of arbitrary load case M-A-B-C: Unloading with constant damage (towards origin) and reloading with damage of loading process below the monotonic curve (towards σ_f).

In order to determine the cyclic damage an arbitrary load case is considered, see Figure 2 (b). After unloading from point M on the monotonic curve, the fiber enters cyclic loading. The residual fracture energy for a point

j is given by the residual fracture energy at the onset of cyclic loading, here denoted point i, and the accumulated work. A simple linear relationship is proposed

$$G_{F,j}^{res} = G_{F,i}^{res} - k_{fat} \sum W \tag{4}$$

where k_{fat} is the fatigue damage parameter. The fatigue damage parameter is a key calibration parameter of the model and is used to scale the fracture energy dissipated during fatigue loading as a fraction of accumulated work. $\sum W$ is the accumulated work, i.e. for the loading process M-A-B, shown in Figure 2 (a),

$$\sum W = W_{\text{M-A}} + W_{\text{A-B}} \tag{5}$$

The work for a load increment, e.g. $W_{\text{A-B}}$, is found from trapezoidal calculation

$$W_{A-B} = (|w_B - w_A|) \left[\frac{\sigma_B + \sigma_A}{2} \right] \tag{6}$$

Considering a fiber in point C, the work from the loading process M-A-B-C is added to the accumulated work upon reloading from C. Reloading from point C takes place towards the fixed point on the monotonic failure envelope (w_f,σ_f), given as, see Figure 2 (b),

$$\sigma_f = \frac{2G_F^{res}}{w_c} \tag{7a}$$

$$w_f = \frac{\sigma_f - f_t}{a} \tag{7b}$$

The stiffness during cyclic loading depends on whether the cohesive surface opens or closes, i.e.

$$\dot{\sigma} = \begin{cases} K_s^- \dot{w} & \text{for} \quad \dot{w} < 0 \\ K_s^+ \dot{w} & \text{for} \quad \dot{w} > 0 \end{cases} \tag{8}$$

where K_s^- and K_s^+ are the unloading and reloading stiffnesses, respectively;

$$K_s^- = \frac{\sigma_u}{w_u} \tag{9a}$$

$$K_s^+ = \frac{\sigma_f - \sigma_r}{w_f - w_r} \tag{9b}$$

where σ_u and σ_r are the stresses at the onset of unloading and reloading, respectively, and w_u and w_r are the crack-openings at the onset of unloading and reloading, respectively.

The stress during unloading and reloading is then given as

$$\sigma = \begin{cases} K_s^- w & \text{for} \quad \dot{w} < 0 \\ K_s^+ \left(w - w_r\right) + \sigma_r & \text{for} \quad \dot{w} > 0 \end{cases} \tag{10}$$

3. Functionality of fatigue model

The proposed methodology is tested and compared to fatigue tests of cracked plain concrete cylinders in uni-axial tension reported in Plizzari et al. [7]. Cylinders with a length of 210 mm, diameter of 80 mm and a notch depth of 4 mm was considered. The crack mouth opening displacement was measured over a length of 35 mm. In these tests only the cracked phase was considered and they are therefore suitable for comparison with the proposed cyclic cohesive model, see example in Figure 3.

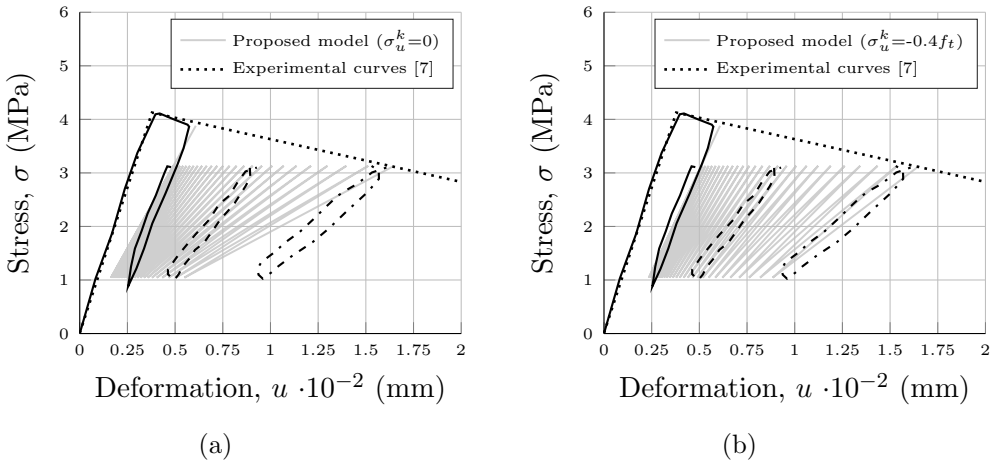

Figure 3: The proposed cyclic cohesive model (gray) compared to fatigue cracking hysteresis loops at the start (black solid), intermediate (black dashed) and end of fatigue analysis (black dashed dotted) reported in [7]: (a) unloading towards origin (σ_u^k=0) and (b) unloading towards σ_u^k=-0.4f_t for load cycles $N : [1 - 280 - 480...5080]$. Specimen geometry (L/d): 210 × 80 × 50 mm^3, notch depth, a_0=4 mm and s=35 mm. Mechanical properties:f_c=42.1 MPa, f_t=4.25 MPa, G_F=151 N/m, w_c=0.341 mm.

From Figure 3 (a) it is observed that the proposed secant unloading scheme does not comply perfectly with experimental curves due to the secant unloading scheme selected. However, it was proposed in [23] to define a fixed negative intersecting point σ_u^k of -0.4f_t on the ordinate, for which results are shown in Figure 3 (b). In this model the parameter σ_u^k is fitted and the response simplified, i.e. this model does not take into account the stiffening of concrete in the tension-compression transition, see e.g. [5, 13, 6] for analytical models and [34, 35] for more advanced concrete damage plasticity formats. With these modifications the model format proposed is suitable for more precise prediction of the concrete cyclic response. Extension of the model to account for unloading towards σ_u^k is presented in Appendix A.

In the three experiments evaluated, the fatigue damage parameter k_{fat} is fitted to $3.4 \cdot 10^{-3}$, $2.2 \cdot 10^{-3}$ and $0.3 \cdot 10^{-3}$ for failure after 344, 645 and 5081 load cycles, respectively. The fitted values are based on the assumption that a specimen fails in fatigue when the reloading curve re-joins the monotonic envelope after undergoing stress controlled fatigue loading. The scatter in these values is mainly related to the variation of concrete tensile strength measured to app. 2.4, 3.7 and 4.3 MPa in the three experiments, respectively.

The study in [7] is one of very few studies in the literature which report data suitable for evaluation of cyclic concrete material behaviour at constitutive level. Thus, the experimental basis for evaluation of the fatigue damage parameter k_{fat} is limited at present. In order to further evaluate the proposed method, or fatigue crack growth phenomena in general, more extensive fracture testing are required.

4. The mechanics of the fiber-hinge model

For analysis of bending in beam structures, the proposed uni-axial cyclic cohesive model in Section 2 is incorporated into a hinge model. The basic assumption of the hinge model is the fact that the presence of a crack influences the overall stress and strain field of a structure only locally. The discontinuity created by the crack is expected to vanish outside a certain width. The width s between two such sections embracing one crack defines a hinge. The hinge width s is a fundamental calibration parameter of the model, and it was suggested by Ulfkjær et al. [24] to use a hinge width half the height of the beam, which is also adopted in the present study.

In the present study the hinge formulation proposed by Skar et al. [23] is applied. This hinge consists of fibers of concrete material, shown in Figure 4.

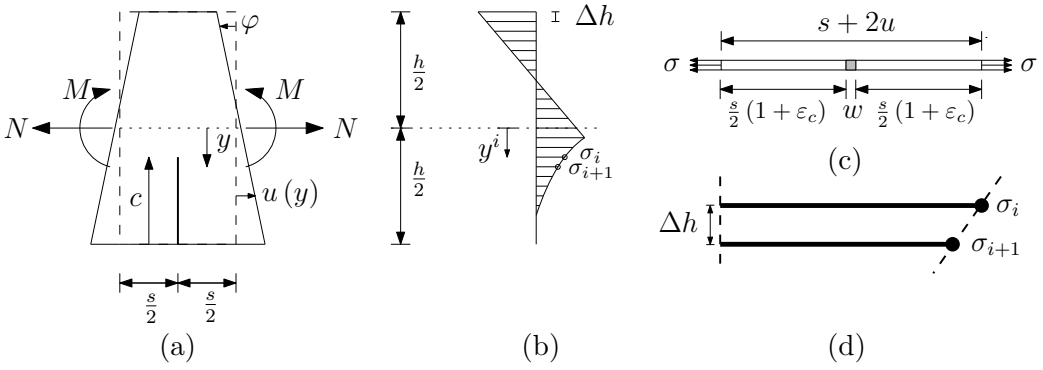

Figure 4: Fiber hinge model: (a) Beam segment with constant sectional forces and deformation of cracked beam segment. (b) Hinge stress distribution after initiation of cracking showing the individual fibers (n=24, whereof 4 stress free). (c) Material fiber in uni-axial tension: loaded state beyond peak-load showing crack deformations. (d) Geometrical definition of one hinge strip (interpolation of stresses between two fibers). From Skar et al. [23].

The tensile behaviour of the hinge may be established by considering a fiber of material in uni-axial tension as shown in Figure 4 (c). The elongation of the fiber located at y can be expressed in terms of the mean normal strain, i.e. $\bar{\varepsilon}(y) = \bar{\varepsilon}_0 + \bar{\kappa} y$. Where $\bar{\varepsilon}_0$ is the mean normal strain at the beam axis, and $\bar{\kappa}$ the mean curvature of the hinge. In the cracked state, the crack opening and the corresponding stress in the fiber are given as

$$\begin{aligned} w_i &= s\frac{E_c\bar{\varepsilon}(y) - f_t}{E_c + as} \quad , \quad \sigma_i = E_c\frac{f_t + as\bar{\varepsilon}(y)}{E_c + as} \quad \text{for} \quad 0 < w_i \leq w_c \\ w_i &= s\bar{\varepsilon}(y) \quad , \quad \sigma_i = 0 \quad \text{for} \quad w_c \leq w_i \end{aligned} \tag{11}$$

The hinge is divided into, $n+1$, number of fibers with the strip height Δh between fibers, shown in Figure 4 (b). The sectional forces with respect to $y = 0$ are then a sum of the contributions from all, n, strips and may be calculated from

$$N(\bar{\varepsilon}_0, \bar{\kappa}) = t \int_{-h/2}^{h/2} \sigma_c \, \mathrm{d}y = \sum_{i=1}^{n} N_i \tag{12a}$$

$$M(\bar{\varepsilon}_0, \bar{\kappa}) = t \int_{-h/2}^{h/2} \sigma_c y \, \mathrm{d}y = \sum_{i=1}^{n} M_i \tag{12b}$$

where N_i and M_i are the normal force contribution and moment contribution from each strip, respectively.

It was found in [23] that sufficient accuracy of the hinge response can be obtained with app. 10-30 fibers.

5. Cyclic hinge response

The functionality of the proposed cyclic hinge model is tested on a single hinge subjected to 25 cycles (N=25) with hinge mean curvature between 1 and 4 mm^{-1}, as shown in Figure 5.

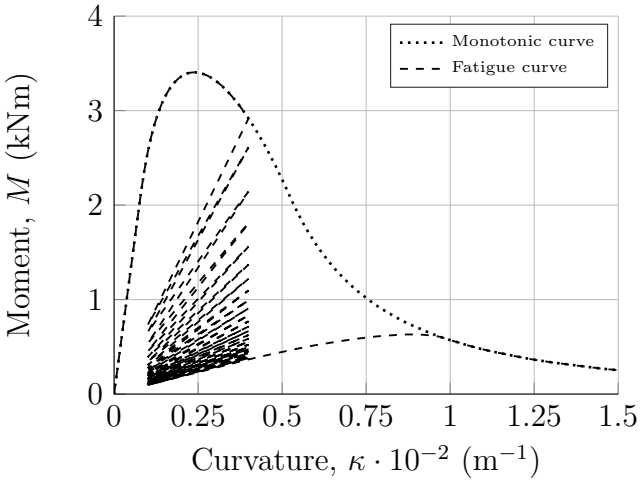

Figure 5: Cyclic behaviour of hinge under constant curvature control: Fatigue damage parameter k_{fat}=0.25. Hinge dimensions (h/t): 0.20 × 0.10 m^2. Hinge parameters: n=50 and s=$H/2$. Material properties: E_c=30 GPa, f_t=3.5 MPa, G_F=150 N/m and w_c=0.1 mm (linear softening).

The evolving stress-mean strain response for the upper quarter hinge fiber, at the position $y = -h/4$, and the bottom hinge fiber, at the position $y = h/2$, during the cyclic loading process is shown in Figure 6 (a) and (b).

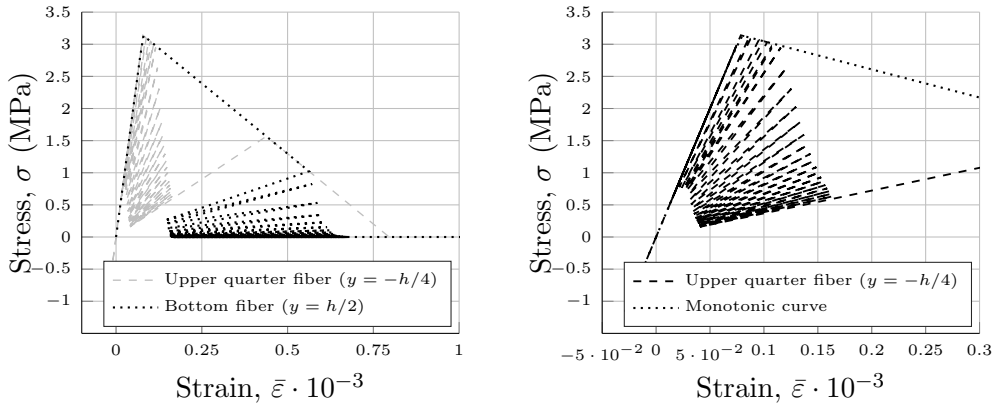

(a) (b)

Figure 6: Behaviour of hinge fibers during cyclic loading: (a) Bottom fiber (black) and upper quarter fiber (gray). (b) Close-up of the upper hinge fiber at position $y = -h/4$ going through different phases during cyclic loading of hinge.

From Figure 6 (a) it is observed that the bottom fiber enters the fatigue phase after the first monotonic load step. As fibers on the lower part of the hinge deteriorate, new fibers in the upper part of the hinge are activated, see Figure 6 (b). The upper hinge fiber is first in compression, then in linear elastic tension, before entering a short stage of low-cyclic monotonic damage, i.e. development of the fracture process zone. Finally, the fiber enters the fatigue phase. This behaviour highlights the importance of a consistent format for numerical simulations of concrete material subjected to cyclic loading, accounting for all the different cracked phases in a unified manner.

6. Implementation of hinge into beam element

The proposed hinge is implemented in a user-built finite element code, hereafter referred to as the FEM hinge. For the present study a plane three-node beam element is chosen, as shown in Figure 7 (a). This element is capable of modelling quadratic variations of the axial displacements and cubic variations of the transverse displacements. The choice of element ensures that both generalized strains are interpolated linearly as opposed to a typical two-node beam element where constant normal strain is assumed. The underlying discrete formulation of cracks for one beam element is shown in Figure 7 (b).

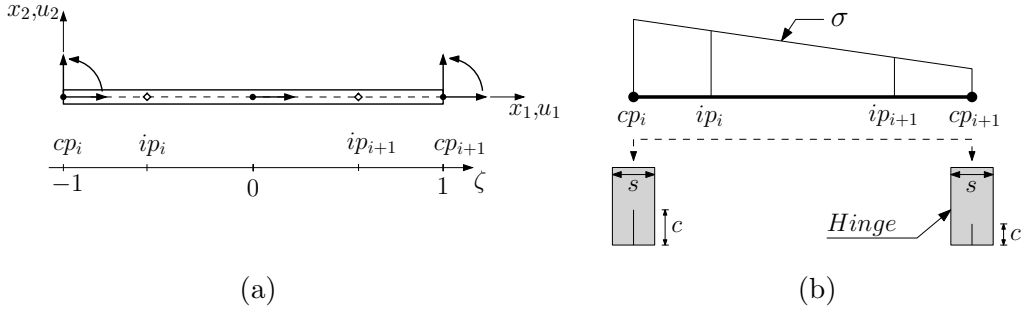

Figure 7: Plane beam element: (a) Constitutive points (cp_i) are located at endpoints, integration points (ip_i) at Gauss points $\pm\sqrt{1/3}$. (b) Underlying discrete formulation of cracks at constitutive points and smeared constitutive behaviour obtained from interpolation between constitutive points at integration points.

The vector of generalized strains, $\boldsymbol{\varepsilon}$, holds the axial strain ε_0 and the

curvature κ. The interpolation of $\boldsymbol{\varepsilon}$ in the element is given by

$$\boldsymbol{\varepsilon} = \begin{bmatrix} \varepsilon_0 \\ \\ \kappa \end{bmatrix} = \begin{bmatrix} \frac{\mathrm{d}u_1}{\mathrm{d}x} \\ \\ \frac{\mathrm{d}^2 u_2}{\mathrm{d}x^2} \end{bmatrix} = \mathbf{B}\boldsymbol{v} \tag{13}$$

where $\mathbf{B}$ is the strain interpolation matrix. The vector of generalized stresses, $\boldsymbol{\sigma}$, holds the sectional normal force N and the sectional moment M and may be established applying (12a) and (12b), i.e. $\boldsymbol{\sigma} = \boldsymbol{\sigma}(\boldsymbol{\varepsilon}) = \begin{bmatrix} N(\boldsymbol{\varepsilon}) \\ M(\boldsymbol{\varepsilon}) \end{bmatrix}$.

The FEM hinge model first determines the constitutive state and stiffness of each individual fiber. Integration over the strip height between fibers is then performed and the sum of all contributions is included in the tangent stiffness matrix. The hinge tangent stiffness matrix, $\mathbf{D}_t$ is defined through

$$\begin{bmatrix} \mathrm{d}N \\ \mathrm{d}M \end{bmatrix} = \mathbf{D}_t \begin{bmatrix} \mathrm{d}\bar{\varepsilon}_0 \\ \mathrm{d}\bar{\kappa} \end{bmatrix} \quad , \quad \mathbf{D}_t = \sum_{i=1}^{n} \begin{bmatrix} \frac{\partial N_i}{\partial \bar{\varepsilon}_0} & \frac{\partial N_i}{\partial \bar{\kappa}} \\ \frac{\partial M_i}{\partial \bar{\varepsilon}_0} & \frac{\partial M_i}{\partial \bar{\kappa}} \end{bmatrix} \tag{14}$$

Monotonic loading of the hinge results in constant positive stiffness of fibers in the linear elastic state. Fibers in the cracked state along the softening branch and cracked stress-free state result in negative and zero stiffness contributions, respectively. The constituents of (14) are obtained from (12a) and (12b) utilising the following relations for the relevant part of the integral $0 < w \leq w_c$

$$\frac{\partial \sigma_c}{\partial \bar{\varepsilon}_0} = E_c \frac{as}{E_c + as} \quad , \quad \frac{\partial \sigma_c}{\partial \bar{\kappa}} = E_c \frac{as}{E_c + as} y \tag{15}$$

Here the parameters $\alpha = \frac{as}{E_c + as}$ and $E_{cc} = E_c \alpha$ are introduced, where the latter symbolizes the reduced stiffness of the cracked fiber. The stiffness contribution from one fiber in the three different phases; elastic, softening

and stress-free is given by (16a), (16b) and (16c), respectively

$$\mathbf{d}_t^{el} = \begin{bmatrix} E_c t & E_c t y \\ E_c t y & E_c t y^2 \end{bmatrix} \qquad \bar{\varepsilon} \leq \bar{\varepsilon}_{ct} \tag{16a}$$

$$\mathbf{d}_t^{cr} = \begin{bmatrix} E_{cc} t & E_{cc} t y \\ E_{cc} t y & E_{cc} t y^2 \end{bmatrix} \qquad \bar{\varepsilon}_{ct} < \bar{\varepsilon} \leq \bar{\varepsilon}_{ult} \tag{16b}$$

$$\mathbf{d}_t^{0} = \begin{bmatrix} 0 & 0 \\ 0 & 0 \end{bmatrix} \qquad \bar{\varepsilon} > \bar{\varepsilon}_{ult} \tag{16c}$$

where $\bar{\varepsilon}_{ult}$ is the ultimate mean strain, i.e. the point where the crack becomes stress-free.

The stiffness contribution from a fiber in the linear elastic state will not change whereas a fiber in the softening state changes from a negative to a positive stiffness. For a fiber during unloading and reloading tensile damage of the fiber is introduced

$$\mathbf{d}_t^{ur} = (1 - \eta)\, \mathbf{d}_t^{el} \qquad \text{for} \quad \bar{\varepsilon}_{ct} < \bar{\varepsilon} < \bar{\varepsilon}_f \tag{17}$$

where $\bar{\varepsilon}_f$ is the mean strain at the monotonic curve, i.e. $\bar{\varepsilon}_f = \sigma_f / E_c + w_f / s$, and η is a damage parameter. The damage parameter η is dependent on whether the crack opens or closes, i.e.

$$\eta = \begin{cases} 1 - \frac{E_s^-}{E_c} & \text{for} \quad \dot{\bar{\varepsilon}} < 0 \\ 1 - \frac{E_s^+}{E_c} & \text{for} \quad \dot{\bar{\varepsilon}} > 0 \end{cases} \tag{18}$$

where E_s^- and E_s^+ are the unloading and reloading stiffnesses, respectively, given by

$$E_s^- = \frac{\sigma_u}{\bar{\varepsilon}_u} \tag{19a}$$

$$E_s^+ = \frac{\sigma_f - \sigma_r}{\bar{\varepsilon}_f - \bar{\varepsilon}_r} \tag{19b}$$

Here σ_u and σ_r are the stresses at the onset of unloading and reloading, respectively, and $\bar{\varepsilon}_u$ and $\bar{\varepsilon}_r$ are the strains at the onset of unloading and reloading, respectively.

The stress during unloading and reloading is given as

$$\sigma = \begin{cases} E_s^- \bar{\varepsilon} & \text{for} \quad \dot{\bar{\varepsilon}} < 0 \\ E_s^+ \left(\bar{\varepsilon} - \bar{\varepsilon}_r\right) + \sigma_r & \text{for} \quad \dot{\bar{\varepsilon}} > 0 \end{cases} \tag{20}$$

The full tangent stiffness matrix for loading, unloading and reloading can now be established by interpolation between each fiber and integration over the strip height, i.e. $\mathbf{D}_t = \int_{-h/2}^{h/2} \mathbf{d}_t \, \mathrm{d}y$, as given in Appendix B. The internal nodal force and the contribution from the beam-element to the tangential stiffness matrix can then be found from standard finite element beam theory.

7. Validation of hinge applied in beam element

The implemented hinge is validated by plotting the moment-curvature behaviour for a single FEM hinge element versus the analytical hinge presented in Section 4. The hinge is subjected to 5 cycles (N=5) with hinge mean curvature between 1 and 4 mm^{-1}, as shown in Figure 8.

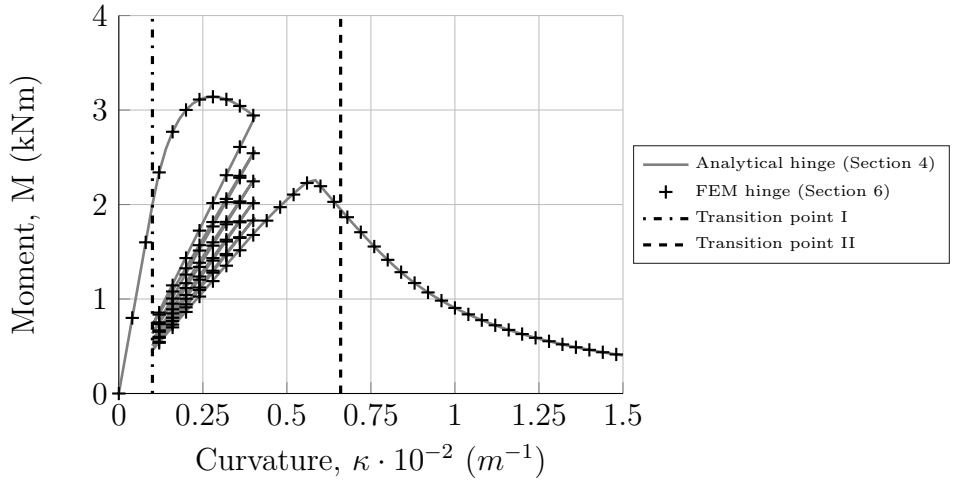

Figure 8: Implementation of hinge into beam element: comparison between analytical and finite element hinge model. Hinge dimensions (h/t): 0.20 × 0.10 m^2. Material properties: E_c=30 GPa, f_t=3.5 MPa, G_F=150 N/m and w_c=0.1 mm (linear softening), k_{fat}=0.25 (linear).

It can be observed from Figure 8 that an exact fit is obtained between the FEM hinge model and analytical model. Fast convergence, within 1-2 iterations, is obtained for this simple model applying a fixed increment of $\Delta\bar{\kappa}$=0.2 mm^{-1}. The two transition points between the phases; elastic-softening (crack initiation) and softening-stress free (bottom fiber stress free) are shown for reference.

8. Fatigue damage of simply supported beam

The proposed model is validated with the results of three point bending beam cyclic tests of plain concrete notched beams, as reported in Toumi et al. [8] and Toumi and Bascoul [36]. Static tests were carried out to obtain an average peak-load, P_u, of 860 $\pm$ 60 N. Cyclic tests were then carried out with a maximum load P_{max} cycled between $0.7P_u$ and $0.98P_u$ with a constant lower load limit, P_{min}, of $0.23P_u$. Beam geometry, material properties and model parameters used are given in Table 1.

Table 1: Geometry and mechanical properties for beams used in experimental studies [36].

Geometry	Unit	Three point beam
Length, L	(m)	0.32
Height, H	(m)	0.08
Thickness, t	(m)	0.05
Notch depth, a_0	(m)	0.04
Mechanical- and fracture properties		
Young's modulus, E	(GPa)	31.6
Tensile strength, f_t	(MPa)	5.2
Fracture energy, G_F	(N/m)	34.2
Hinge model and numerical parameters		
Number of fibers[1], n	(-)	200
Hinge width[2], $s = H/2$	(m)	0.04
Number of elements, *nel*	(-)	6
Fatigue damage parameter, k_{fat}	(-)	$4.6 \cdot 10^{-3}$
Error tolerance, ϵ	(-)	$1 \cdot 10^{-4}$

[1]selected in order to obtain a smooth crack growth curve in Figure 10

[2]as proposed in [24]

In the present study the energy norm ratio $\delta E_1/\Delta E_0 \leq \epsilon$ is applied as a measure in the convergence criterion using a conventional Newton-Raphson (N-R) solver with load control. Here ΔE_0 is the initial energy calculated in the first load step and δE_1 is the energy during iterations based on the residual forces.

In lack of experimental data, the fatigue damage parameter k_{fat} is calibrated to obtain failure at N=140 load cycles, found from experiments for a load level of $0.98P_u$. This value is then used for simulations of the beam subjected to cyclic loads of $0.97P_u$ and $0.93P_u$ without further calibration.

Convergence of the model is evaluated in view of load-displacement behaviour of the beam, plotting the peak-load displacement for different beam mesh densities, *nel*: 2-12, shown in Figure 9 (a). Typical load-displacement behaviour is plotted in Figure 9 (b). In the analytical model, implementing the hinge into an elastic beam as suggested by Olesen [25], only one hinge is considered. This explains the slightly stiffer behaviour compared to the

FEM hinge.

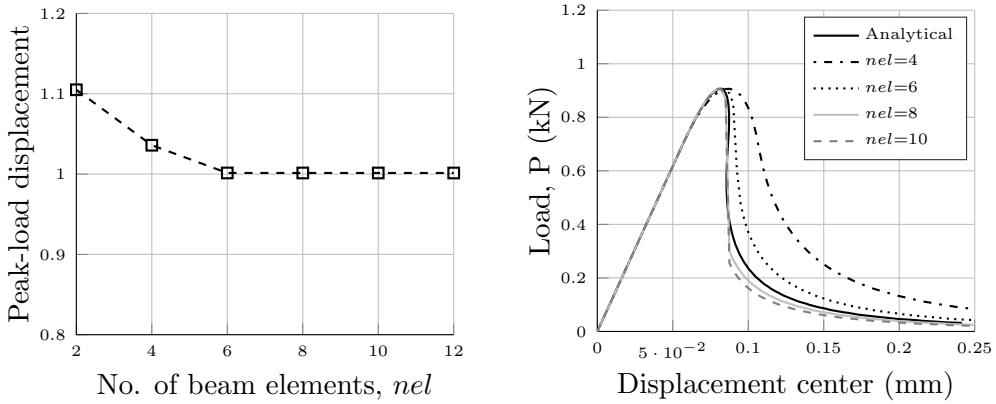

Figure 9: Convergence test: (a) Number of beam elements, nel:2-10 (element size, $elsz$: 0.032-0.16 m) versus peak-load displacement (normalized with regard to the analytical hinge solution) (b) Load-displacement behavior for different mesh densities compared to the analytical hinge solution.

From Figure 9 (b) it is observed, that sufficient accuracy, can be obtained with 6 elements, resulting in an element size of 0.053 m, chosen in the following analysis. From Figure 9 (b) it is observed that the peak-load P_u predicted with the hinge model is app. 900 N. This agrees reasonably well with the average peak load of 860 $\pm$ 60 N that was obtained by [8]. The functionality of the proposed numerical hinge for simulation of the cyclic fracture behaviour of a three point beam in the fatigue phase is demonstrated by plotting crack length versus the number of load cycles with the experimental results, as shown in Figure 10.

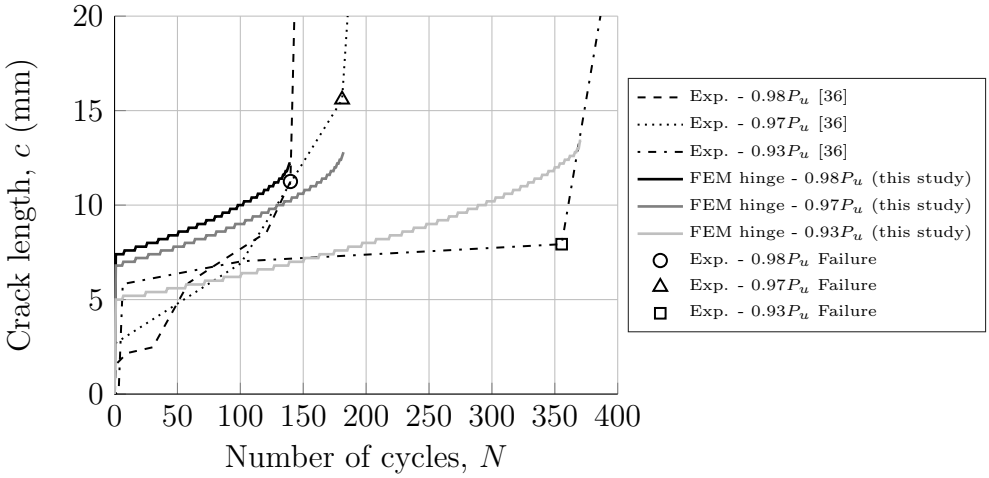

Figure 10: FEM hinge versus experimental and model curves reported in [36]: Crack length versus number of load cycles. Where the crack length c is taken as the progressive depth to the crack tip.

It is observed from Figure 10 (a) that the FEM hinge model is able to capture the fatigue crack growth development during cyclic loading after an initial phase of app. 50 load cycles. Moreover, some characteristic features of the model are shown:

(i) The initial crack length increases with increasing P_{max}.

(ii) The crack growth rate increases with increasing P_{max}.

(iii) The fatigue life increases for decreasing P_{max}.

It is also observed that the numerical crack growth curves for $0.93P_u$ resemble the experimental curves, and that all three models are able to give a close prediction of the number of load repetitions to failure, without further calibration, as shown in Figure 11 (a).

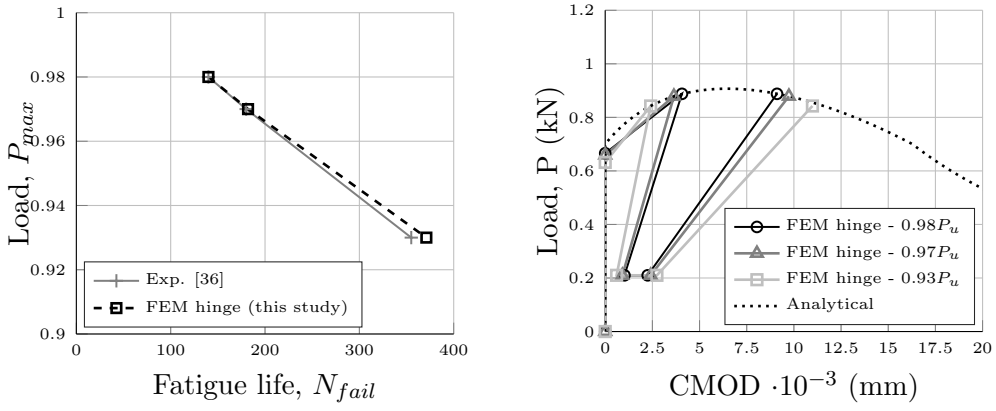

(a) (b)

Figure 11: FEM hinge versus experimental and model curves reported in [36]: (a) Crack length versus number of load cycles comparing numerical and experimental results. (b) Close-up of load-crack mouth opening displacement curve for the FEM hinge model plotting the first and last load cycle during cyclic loading together with the monotonic response.

From the load-crack mouth opening displacement curve in Figure 11 (b) it is observed, that the FEM hinge performs satisfactory, as the point of crack initiation, unloading and failure comply with the analytical monotonic curve.

9. Conclusions

A simple energy based approach for damage evolution during cyclic loading was proposed, requiring only a single model parameter additional to the monotonic parameters. The selected format is general and consistent and ensures that damage during cyclic loading in fatigue is restricted to the monotonic failure envelope, i.e. the damage state after arbitrary loading is associated with a monotonic loading process that leads to the same damage state. The proposed model shows satisfactory results when compared to experiments with cracked plain concrete cylinders in uni-axial tension. Moreover, it can be shown that the model, with simple modifications, is able to resemble the unloading-reloading response of experimental curves.

The use of a cyclic fiber-hinge model for simulating cyclic damage of a concrete beam has been investigated showing good performance. Implementation of the hinge into a beam element is relatively straightforward and the

contribution to the tangent stiffness matrix from each fiber is established following a general format, creating a versatile tool, allowing for different types of softening laws and damage formats.

The finite element hinge adequately describes the fatigue crack growth of plain concrete beams under three point loading. Main characteristic features, such as initial crack length and fatigue crack growth rate, can be simulated with the finite element hinge model. It is found that the energy based methodology applied is able to capture the influence of varying load amplitude, with a close prediction of the number of cycles to failure.

The present paper demonstrates the implementation and application of a cyclic cohesive fiber-hinge model to describe the fatigue fracture behaviour of concrete beam structures. The results obtained are encouraging and show that the methodology is well suited for practical use.

Acknowledgements

The authors would like to thank COWIfonden [grant no. C-123.03] and Innovation Fund Denmark [grant no. 1355-00060] for financial support of the research presented in this paper.

10. References

[1] H. Cornelissen, Fatigue failure of concrete in tension, HERON, 29 (4), 1984.

[2] V. Slowik, G. A. Plizzari, V. E. Saouma, Fracture of concrete under variable amplitude fatigue loading, ACI Materials Journal 93 (1996) 272–283.

[3] K. Gylltoft, Fracture mechanics models for fatigue in concrete structures, Luleå Institute of Technology, Division of Structural Engineering, 1983.

[4] V. S. Gopalaratnam, S. P. Shah, Softening response of plain concrete in direct tension, Journal of the American Concrete Institute, J Am Conc I, J Am Concrete I, J Amer Concr Inst 82 (3) (1985) 310–323.

[5] H. W. Reinhardt, H. A. Cornelissen, D. A. Hordijk, Tensile tests and failure analysis of concrete, Journal of Structural Engineering 112 (11) (1986) 2462–2477.

[6] D. Hordijk, Tensile and tensile fatigue behaviour of concrete; experiments, modelling and analyses, Heron 37 (1) (1992) 1–79.

[7] G. Plizzari, S. Cangiano, S. Alleruzzo, The fatigue behaviour of cracked concrete, Fatigue & Fracture of Engineering Materials & Structures 20 (8) (1997) 1195–1206.

[8] A. Toumi, A. Bascoul, A. Turatsinze, Crack propagation in concrete subjected to flexuralcyclic loading, Materials and Structures 31 (7) (1998) 451–458.

[9] C. Kessler-Kramer, V. Mechtcherine, H. Müller, Fatigue behaviour of concrete in tension, Fracture Mechanics of Concrete Structures, de Borst et al.(eds), Sweets & Zeitlinger, Lisse (2001) 573–578.

[10] J. Zhang, H. Stang, V. C. Li, Fatigue life prediction of fiber reinforced concrete under flexural load, International Journal of Fatigue 21 (10) (1999) 1033–1049.

[11] J. Zhang, H. Stang, V. C. Li, Experimental study on crack bridging in frc under uniaxial fatigue tension, Journal of Materials in Civil Engineering 12 (1) (2000) 66–73.

[12] K. Gylltoft, A fracture mechanics model for fatigue in concrete, Matériaux et Construction 17 (1) (1984) 55–58.

[13] D. Z. Yankelevsky, H. W. Reinhardt, Response of plain concrete to cyclic tension, Materials Journal 84 (5) (1987) 365–373.

[14] H. Horii, H. Shin, T. Pallewatta, An analytical model of fatigue crack growth in concrete, Proc Jpn Concr Inst 12 (1990) 835–840.

[15] J. Elias, J.-L. Le, Modeling of mode-i fatigue crack growth in quasibrittle structures under cyclic compression, Engineering Fracture Mechanics 96 (2012) 26–36. doi:10.1016/j.engfracmech.2012.06.019.

[16] O. Nguyen, E. Repetto, M. Ortiz, R. Radovitzky, A cohesive model of fatigue crack growth, International Journal of Fracture 110 (4) (2001) 351–369. doi:10.1023/A:1010839522926.

[17] B. Yang, S. Mall, K. Ravi-Chandar, A cohesive zone model for fatigue crack growth in quasibrittle materials, International Journal of Solids and Structures 38 (22) (2001) 3927–3944.

[18] K. Roe, T. Siegmund, An irreversible cohesive zone model for interface fatigue crack growth simulation, Engineering Fracture Mechanics 70 (2) (2003) 209–232. doi:10.1016/S0013-7944(02)00034-6.

[19] M. Ortiz, A. Pandolfi, Finite-deformation irreversible cohesive elements for three-dimensional crack-propagation analysis, International Journal for Numerical Methods in Engineering 44 (9) (1999) 1267–1282.

[20] S. Roth, G. Hütter, M. Kuna, Simulation of fatigue crack growth with a cyclic cohesive zone model, International Journal of Fracture 188 (1) (2014) 23–45.

[21] M. Kuna, S. Roth, General remarks on cyclic cohesive zone models, International Journal of Fracture 196 (1-2) (2015) 147–167.

[22] A. Hillerborg, M. Modéer, P.-E. Petersson, Analysis of crack formation and crack growth in concrete by means of fracture mechanics and finite elements, Cement and concrete research 6 (6) (1976) 773–781.

[23] A. Skar, P. N. Poulsen, J. F. Olesen, General cracked-hinge model for simulation of low-cycle damage in cemented beams on soil, Engineering Fracture Mechanics 175 (2017) 324–338. doi:10.1016/j.engfracmech.2017.01.016.

[24] J. P. Ulfkjær, S. Krenk, R. Brincker, Analytical model for fictitious crack propagation in concrete beams, Journal of Engineering Mechanics 121 (1) (1995) 7–15.

[25] J. F. Olesen, Fictitious crack propagation in fiber-reinforced concrete beams, Journal of Engineering Mechanics 127 (3) (2001) 272–280. doi:10.1061/(ASCE)0733-9399(2001)127:3(272).

[26] J. Zhang, V. C. Li, H. Stang, Size effect on fatigue in bending of concrete, Journal of materials in civil engineering 13 (6) (2001) 446–453.

[27] N. A. Brake, K. Chatti, Prediction of size effect and non-linear crack growth in plain concrete under fatigue loading, Engineering Fracture Mechanics 109 (2013) 169–185.

[28] A. Carpinteri, Energy dissipation in rc beams under cyclic loadings, Engineering Fracture Mechanics 39 (2) (1991) 177–184.

[29] J. F. Olesen, Cracks in reinforced frc beams subject to bending and axial load, Fracture mechanics of concrete structures, vols 1 and 2 (2001) 1027–1033.

[30] A. Carpinteri, A. Spagnoli, S. Vantadori, A fracture mechanics model for a composite beam with multiple reinforcements under cyclic bending, International Journal of Solids and Structures 41 (20) (2004) 5499–5515.

[31] A. Carpinteri, A. Spagnoli, S. Vantadori, An elastic–plastic crack bridging model for brittle-matrix fibrous composite beams under cyclic loading, International Journal of Solids and Structures 43 (16) (2006) 4917–4936.

[32] J. F. Olesen, P. N. Poulsen, Modeling rc beam structures based on cracked hinge model and finite elements, Tech. Rep. SR12-11, Technical University of Denmark, DTU Civil Engineering (2012).

[33] A. Skar, P. N. Poulsen, J. F. Olesen, Cohesive cracked-hinge model for simulation of fracture in one-way slabs on grade, International Journal of Pavement Engineering 0 (0) (0) 1–15. doi:10.1080/10298436.2017.1293263.

[34] J. Lee, G. Fenves, Plastic-damage model for cyclic loading of concrete structures, Journal of Engineering Mechanics 124 (8) (1998) 892–900.

[35] P. Grassl, D. Xenos, U. Nyström, R. Rempling, K. Gylltoft, Cdpm2: A damage-plasticity approach to modelling the failure of concrete, International Journal of Solids and Structures 50 (24) (2013) 3805–3816.

[36] A. Toumi, A. Bascoul, Mode i crack propagation in concrete under fatigue: microscopic observations and modelling, International journal for numerical and analytical methods in geomechanics 26 (13) (2002) 1299–1312.

Appendix A. Extended fatigue model

The proposed fatigue model can be extended to account for unloading towards a fixed negative point on the ordinate. The initial unloading stiffness is expressed as

$$K_s^- = \frac{\sigma_u - \sigma_u^k}{w_u} \tag{A.1}$$

where σ_u is the stress and w_u is the crack-opening displacement at the onset of unloading, respectively, and σ_u^k is the fixed negative intersecting point on the ordinate.

The crack-opening displacement at the point where the unloading curve intersect with the abscissa is given by

$$w_0 = \frac{\sigma_u^k}{K_s^-} \tag{A.2}$$

The dissipated energy from the monotonic crack-opening process, the reversible elastic and residual fracture energy upon the first fatigue load cycle in (3a)-(3c) can then be reformulated as

$$E^{rev} = \frac{1}{2}\sigma_u \left(w_u - w_0\right) \tag{A.3a}$$

$$E_{mon}^{dis} = \frac{1}{2}\left(\sigma_u - \sigma_u^k\right) w_u - \frac{1}{2}\sigma_u^k w_0 \tag{A.3b}$$

$$E^{res} = \frac{1}{2}\sigma_u \left(w_c - w_u\right) \tag{A.3c}$$

where w_u is the crack-opening at the onset of unloading, σ_u is the stress at the onset of unloading and w_c is the final zero-stress crack-opening.

Appendix B. Derivation of hinge tangent stiffness matrix

Interpolation between hinge fibers and integration over the strip height is given as

$$\begin{aligned}
\mathrm{d}N_i &= \left(\int_{y_i}^{y_{i+1}} \frac{1}{2} \left(d_{11}^i + d_{12}^{i+1} \right) \, \mathrm{d}y \right) \mathrm{d}\bar{\varepsilon}_0 + \left(\int_{y_i}^{y_{i+1}} \frac{1}{2} \left(d_{12}^i + d_{12}^{i+1} \right) \, \mathrm{d}y \right) \mathrm{d}\bar{\kappa} \\
&= \left(\frac{1}{2} \left(d_{11}^i + d_{11}^{i+1} \right) (y_{i+1} - y_i) \right) \mathrm{d}\bar{\varepsilon}_0 \\
&\quad + \left(\frac{1}{2} \left(d_{12}^i + d_{12}^{i+1} \right) (y_{i+1} - y_i) \frac{1}{2} (y_i + y_{i+1}) \right) \mathrm{d}\bar{\kappa} \\
&= d_{11}^i \, \mathrm{d}\bar{\varepsilon}_0 + d_{12}^i \, \mathrm{d}\bar{\kappa} \\
&= \frac{\partial N_i}{\partial \bar{\varepsilon}_0} \, \mathrm{d}\bar{\varepsilon}_0 + \frac{\partial N_i}{\partial \bar{\kappa}} \, \mathrm{d}\bar{\kappa}
\end{aligned} \tag{B.1a}$$

$$\begin{aligned}
\mathrm{d}M_i &= \left(\int_{y_i}^{y_{i+1}} \frac{1}{2} \left(d_{21}^i + d_{21}^{i+1} \right) \, \mathrm{d}y \right) \mathrm{d}\bar{\varepsilon}_0 + \left(\int_{y_i}^{y_{i+1}} \frac{1}{2} \left(d_{22}^i + d_{22}^{i+1} \right) \, \mathrm{d}y \right) \mathrm{d}\bar{\kappa} \\
&= \left(\frac{1}{2} \left(d_{21}^i + d_{21}^{i+1} \right) (y_{i+1} - y_i) \frac{1}{2} (y_i + y_{i+1}) \right) \mathrm{d}\bar{\varepsilon}_0 \\
&\quad + \left(\frac{1}{2} \left(d_{22}^i + d_{22}^{i+1} \right) (y_{i+1} - y_i) \frac{1}{3} \left(y_i^2 + y_{i+1}^2 + y_i y_{i+1} \right) \right) \mathrm{d}\bar{\kappa} \\
&= d_{21}^i \, \mathrm{d}\bar{\varepsilon}_0 + d_{22}^i \, \mathrm{d}\bar{\kappa} \\
&= \frac{\partial M_i}{\partial \bar{\varepsilon}_0} \, \mathrm{d}\bar{\varepsilon}_0 + \frac{\partial M_i}{\partial \bar{\kappa}} \, \mathrm{d}\bar{\kappa}
\end{aligned} \tag{B.1b}$$

where y_i and y_{i+1} are the position of each fiber depicted on Figure 4 and d_{11}, d_{12}, d_{21} and d_{22} is defined in (16) as $\mathbf{d}_t = \left[\begin{smallmatrix} d_{11} & y\, d_{12} \\ y\, d_{21} & y^2\, d_{22} \end{smallmatrix} \right]$.

The sum of all contributions is included in the tangent stiffness matrix similar to (14), i.e.

$$\mathbf{D}_t = \sum_{i=1}^{n} \begin{bmatrix} \frac{\partial N_i}{\partial \bar{\varepsilon}_0} & \frac{\partial N_i}{\partial \bar{\kappa}} \\ \frac{\partial M_i}{\partial \bar{\varepsilon}_0} & \frac{\partial M_i}{\partial \bar{\kappa}} \end{bmatrix} \tag{B.2}$$